ROYAL SOCIETY
OF CHEMISTRY

COMMUNICATION

An extremely thin and robust interconnecting layer providing 76% fill factor in a tandem polymer solar cell architecture†

Alberto Martínez-Otero,*[a] Quan Liu,[a] Paola Mantilla-Perez,[a] Miguel Montes Bajo[a] and Jordi Martorell[ab]

We report a thin and robust interconnecting layer (ICL) for polymer tandem solar cells. This ICL shows low absorption, good electrical contacts, large work function contrast and robustness. Its use yields tandem cells with a very high fill factor of 76%, making this ICL a promising component of future highly efficient multijunction organic solar cells.

Bulk heterojunction polymer solar cells represent a promising technology which could be an important player in the future photovoltaic market due to their light weight, flexibility, semi-transparency, low cost, and rapid energy payback time.[1–6] The power conversion efficiency (PCE) of these polymer solar cells (PSCs) has been improved markedly in recent years[7–10] and has now exceeded the milestone value of 10%,[11] which makes their industrialization to eventually commercialize them very promising. Moreover, by using the tandem concept,[12] in which two or more subcells with complementary absorption spectra are stacked on top of each other and connected in series or parallel configuration, the PCE has been recently boosted to near 11%.[13] Yang *et al.* and Brabec *et al.* recently published articles on organic single and tandem solar cells providing comprehensive reviews of different device structures and their working mechanisms.[14,15] Several studies foresee that there is still room for improvement. Dennler *et al.* predicted that organic tandem solar cells comprising two series-connected single junction cells would be able to reach a PCE of 15% assuming 65% fill factor (FF) and a constant External Quantum Efficiency (EQE) of 65%.[16] At present, those assumptions should be revised due to the fruitful and extensive research done in the last few years developing and optimizing buffer layers, donor materials and morphology. Recently, the same group predicted that organic

tandem devices can reach 21% efficiency assuming 80% EQE and 75% FF.[17] Recently, Facchetti *et al.* reported a new donor polymer with high performance and a FF approaching values of their inorganic counterparts.[18]

The FF characterizes how "rectangular" the J–V curve is and it represents how "difficult" or "easy" the photogenerated carriers can be extracted out of a photovoltaic device. This parameter is crucial to determine the performance of an organic solar cell together with the short circuit current density (J_{sc}) and the open-circuit voltage (V_{oc}). There are several factors that can influence the FF in a complex way, thus making the FF one of the least understood parameters among the ones determining the PCE.[19]

Commonly, in the fabrication of PSCs, several actions have shown to be beneficial for improving the FF and hence the efficiency like, for instance, improving the morphology[20,21] or choosing appropriate buffer layers that can help diminish the contact resistance (reduce R_s) or the current leakage (increase R_{sh}).[22]

The buffer layers normally used as transporting layers in single junction solar cells also play another important role in multijunction solar cells as they are commonly part of the interconnecting layer (ICL). In tandem cells, the ICL serves as the charge recombination zone between the front and rear subcells; the ICL is vital in realizing high performance in tandem cells.[23] Further requirements of the ICL are transparency and robustness to protect the underlying layers against damage from further solution processing of the rear subcell.

In this study, we report a novel and very thin ICL for multijunction configurations which provides FFs exceeding the ones of the single cells forming part of it and reaching values up to 76%, never reported before in organic tandem solar cells to the best of our knowledge. Herein, we employed a MoO_3/Ag/PFN ICL layer, less than 20 nm thick, connecting two identical, inverted PTB7:PC71BM subcells in series. By using identical polymers in both subcells, one can overcome the decrease in J_{sc}, FF, and ultimately PCE usually observed in single-junction cells when the thickness of the active layer is increased (see Fig. S1

[a]*ICFO – The Institute of Photonic Sciences, Av. Carl Friedrich Gauss, 3, 08860 Castelldefels, Barcelona, Spain. E-mail: a.martinez.otero@fz-juelich.de*

[b]*Departament de Física i Enginyeria Nuclear, Universitat Politècnica de Catalunya, 08222 Terrassa, Spain*

This journal is © The Royal Society of Chemistry 2015

J. Mater. Chem. A, 2015, **3**, 10681–10686 | **10681**

and S2, ESI†). Indeed, a transfer matrix-based numerical determination of light absorption[24,25] predicts a 14% increase in J_{sc} for the same polymer tandem cells relative to the optimal single-junction cell. The more commonly used PEDOT and ZnO ICL materials need thermal treatments that, despite efforts to decrease their temperature (see, for example, ref. 26), may still be detrimental to the bottom organic layers. Moreover, this ICL was used to have a thickness around 100 nm also to protect the underneath layers. Accordingly, in the device architecture described below, we employed thin layers of thermally evaporated MoO_3 and the conjugated polyelectrolyte poly[9,9-bis(3′-(N,N-dimethylamino)propyl)-2,7-fluorene]-alt-2,7-(9,9-dioctylfluorene)] (PFN) that can be deposited from solution without any further treatment. A thin Ag layer was evaporated between those two layers in order to favour the recombination of charges. In a recent report by Zheng et al., a similar ICL was employed and 0.5 nm of Ag were also used to establish ohmic contact.[11]

It is also worth mentioning that only a few nanometers of PFN were necessary to obtain a good electrical contact and to protect the underlying layers from solvent penetration upon the deposition of the top subcell. As a result, the FF of the PTB7:PC71BM system was increased to a value of 76% in the tandem solar cells, never reported before to the best of our knowledge, while the PCE was increased from 7.3% in a single junction to 8.2% in our best tandem cells.

The tandem device structure used here is shown in Fig. 1 as well as the chemical structures of the PTB7 and PFN polymers and the device band structure. Two inverted cells with the same donor–acceptor materials were used, with the donor material being the well-known benzodithiophene derivative PTB7.[27] The use of the same active blend in both subcells of a tandem cell has been considered in the past by You et al. Their research led to the same polymer tandem cell with 10.2% PCE. It is noticeable that, with a thick ICL, the FF they obtained was 65%.[28] Recently it has been shown by our group, for a four terminal configuration tandem device of the same material, that optical optimization of the field distribution is essential to obtain optimized light harvesting and to overcome the absorption capacity of the single layered cell (paper to be published) which is limited by the charge mobility in the active blend.

In contrast to other related studies, our tandem solar cell is composed of two subcells with different electron transporting layers (ETL). In the case of the front cell, a sol–gel solution of ZnO was used while for the rear cell, a PFN layer was deposited by spin coating.

In previous studies by our group, we were able to enhance the photovoltaic properties of the PTB7:PC71BM system using direct structures.[5,24] In the current work, we fabricated inverted structures of the PTB7:PC71BM blend due to its better stability as there is no need to use the acidic PEDOT:PSS.[29]

We investigated the photovoltaic performance of single junction inverted PTB7:PC71BM PSCs with the following configurations, SJ1: glass/ITO/ZnO/PTB7:PC71BM/MoO_3/Ag and SJ2: glass/ITO/PFN/PTB7:PC71BM/MoO_3/Ag. The single junction device of type SJ1 yields a V_{oc} = 0.74 V, a J_{sc} = 14.3 mA cm^{-2} and a FF = 69%, resulting in a PCE = 7.3% for a blend thickness of ca. 100 nm and a ZnO thickness of 35 nm. The same PCE could be obtained for a device of type SJ2 which exhibited a V_{oc} = 0.72 V, a J_{sc} = 14.3 mA cm^{-2} and a FF = 71% for a blend thickness of ca. 100 nm and a PFN thickness of 12 nm. The blend composed of PTB7:PC71BM dissolved in chlorobenzene (CB) was deposited inside a glovebox to a thickness of ca. 100 nm in both cases. After a vacuum-drying period, the top electrode was evaporated on both devices, composed of 3 nm of MoO_3 followed by 100 nm of Ag. After fabrication, all measurements were carried out in air without encapsulation and showed very similar results for both inverted structures. Device performances are summarized in Table 1. Some differences can be seen from the EQE data of both SJ1 and SJ2 devices, especially in the 400 nm to 600 nm region of the spectra (Fig. S3, ESI†). In any case, the theoretical current densities extracted from the type SJ1 and SJ2 graphs are very similar between them and in accordance with the experimental results obtained. The EQE of the SJ2 device with PFN is rather featureless between 500 nm and 700 nm and shows an average value of 65%. For the SJ1 device, with ZnO, peaks of 68% are observed at around 480 nm and in the 620 nm to 680 nm range. Around 400 nm and 550 nm, the EQE values of the SJ1 device are lower than those of the PFN. Such differences arise mostly because of the dissimilar extinction coefficients of the transporting layers that modify the field distribution inside the device.
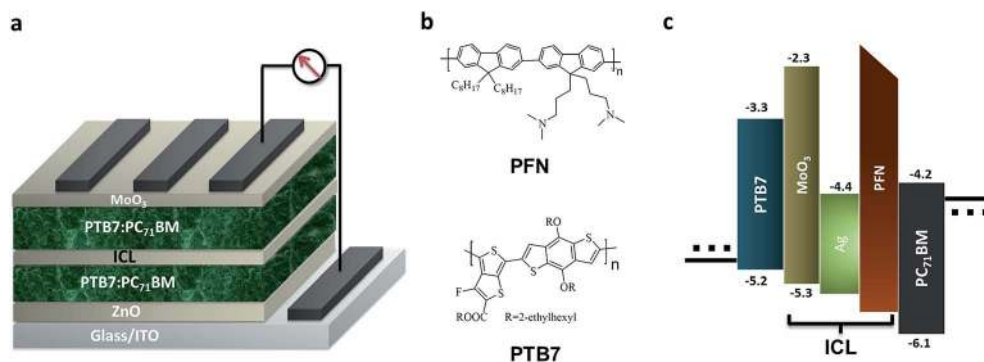

Fig. 1 (a) Device configuration of the tandem solar cell with a MoO_3/Ag/PFN interconnecting layer. (b) Chemical structure of the donor polymer PTB7 and conjugated polyelectrolyte PFN. (c) Schematic of the device band alignment.

10682 | J. Mater. Chem. A, 2015, 3, 10681–10686

This journal is © The Royal Society of Chemistry 2015

Table 1 Performance parameters of the single junction devices with different ETL and tandem devices with best efficiency and record FF. Single junction devices: glass/ITO/ETL/PTB7:PC$_{71}$BM/MoO$_3$/Ag where SJ1 uses ZnO and SJ2 uses PFN as an ETL. Error bars are the standard deviation from the average values. Tandem devices: glass/ITO/ZnO/ PTB7:PC$_{71}$BM/MoO$_3$/Ag/PFN/PTB7:PC$_{71}$BM/MoO$_3$/Ag. Average values (±standard deviation) for the PCE and FF of the tandem cells are 8.0 ± 0.2% and 73.8 ± 1.5%, respectively

Device	J_{sc} [mA cm^{-2}]	V_{oc} [mV]	PCE [%]	FF [%]
SJ1	14.3 ± 0.2	741 ± 0.003	7.3 ± 0.1	69 ± 0.4
SJ2	14.3 ± 0.3	723 ± 0.002	7.3 ± 0.1	71 ± 1
T1 (best PCE)	7.6	1480	**8.2**	73
T2 (best FF)	6.9	1477	7.8	**76**

The tandem solar cell devices (type T) incorporating our new robust ICL show the following configuration: glass/ITO/ZnO/ PTB7:PC71BM/MoO$_3$/Ag/PFN/PTB7:PC71BM/MoO$_3$/Ag.

It is well known that in a series-connected tandem solar cell, the photocurrents generated by the subcells have to be balanced to maximize the device performance. The optical simulation has been proven to be a powerful and reliable method to optimize the layer sequence as well as the layer thickness of tandem solar cells by calculating the photocurrents of both subcells.[30] After the effective refractive index and thickness of the different layers were obtained, we implemented an optical simulation by means of the transfer matrix method to numerically determine the optimal device architecture following an inverted problem-solving procedure. More details about the optical model employed can be found in ref. 24 and 25.

As a summary of this numerical study, in Fig. 2a, the dependence of J_{sc} on the thickness of the front and rear active layers of the tandem solar cell is shown. All the thicknesses of the other conforming layers in the tandem cell are kept constant. As observed in such a current map, having a front subcell with a thickness between 80 nm and 110 nm in combination with a rear subcell with a thickness between 90 nm and 130 nm leads to the optimal values of the current density. In contrast, lower current values arise when the front cell thickness reaches above 110 nm, because the rear subcell

current becomes a significant limiting factor. Lower current values also arise when the two subcells are below 90 nm. The tendency observed in Fig. 2a shows that the current maxima can also be found for thicker rear subcells, above 130 nm, but these cases are not desirable from the electrical point of view because of the lower performance of solar cells with increasing thickness.[28] For this reason, we kept the rear subcell in our devices with thicknesses around 120 nm. Even if they are not in the highest current region, we could achieve 7.6 mA cm^{-2} for our best device, which approximates to the largest possible current of 7.8 mA cm^{-2} according to our simulations. The thicknesses of the active layers of this device could be measured by means of an atomic force microscope (AFM; see ESI Fig. S4†) showing values of 100 nm for the front subcell and 117 nm for the rear subcell. As indicated, a J_{sc} = 7.6 mA cm^{-2}, a V_{oc} = 1.48 V and a FF = 73%, resulting in a PCE = 8.2%, were obtained for our best performance tandem solar cell, and a V_{oc} = 1.48 V, a J_{sc} = 6.9 mA cm^{-2} and a FF = 76%, resulting in a PCE = 7.8%, were obtained for our best FF tandem solar cell with front and rear subcell thicknesses of 106 nm and 122 nm, respectively.

For comparison, the experimentally determined FF values of PTB7:PC71BM single-junction cells were found to decrease with increased active layer thickness. For an active layer thickness equivalent to the sum of those of the FF = 76% tandem cell subcells taken together (i.e. active layer thickness 228 nm) it is found that FF < 61%. Therefore, the stacked tandem approach results in an FF increase of ~25% (see Fig. S1b, ESI†). The J–V curves of the type T devices can be seen in Fig. 2 together with the SJ1 and SJ2 devices. Device performances are also summarized in Table 1.

In order to verify the robustness of our ICL, we used it in a tandem cell configuration composed of a front subcell of P3HT and a rear subcell of PTB7. Results can be seen in the ESI.† Even though the configuration was not optically or electrically optimized, the tandem cell presented a FF 8% higher than the highest FF measured for any of the two subcells (Fig. S5, ESI†).

A more in depth study was performed on our new ICL; in Fig. 3a, the measured extinction coefficient (k) values of MoO$_3$ and PFN are shown. The sol–gel processed ZnO used as an ETL in the front subcell is also included. Both ZnO and MoO$_3$ have
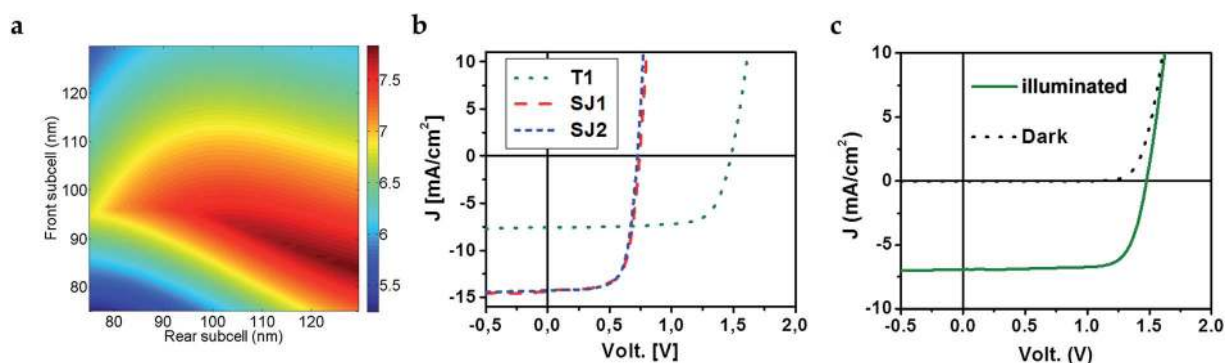

Fig. 2 (a) Simulated current density generated in a tandem solar cell device as a function of the front and rear active layers. (b) J−V characteristics of devices SJ1, SJ2 (single junction solar cells) and T1 (tandem solar cell with best efficiency) under AM1.5 100 mW cm^{-2} illumination. (c) J−V characteristics of device T2 (tandem solar cell with record FF) in the dark and under AM1.5 100 mW cm^{-2} illumination.

practically no absorption in the visible region, values of k equal to 0 from 400 nm onwards, while the PFN displays a sharp narrow peak at 400 nm.

In accordance with the k values of the materials, we can see in Fig. 3b that the absorptance of MoO_3 in glass is negligible. If 1 nm of Ag is evaporated on top of the MoO_3, a short broad peak appears at around 540 nm and finally when a thin film of PFN is spin-coated on top, to complete the ICL, a sharp peak at 400 nm appears together with the broad one observed for silver. On average, we were able to obtain a rather transparent interlayer as can be seen from the absorptance spectra of the ICL deposited on glass. Also, the PFN layer reduces the roughness of the MoO_3/Ag layer to an RMS of 0.8 nm as observed by AFM (see Fig. S6, ESI†).

We also constructed the following device structure: ITO/ MoO_3/Ag/PFN/Ag and measured the J–V response before and after UV illumination (see Fig. S7, ESI†). The linear response suggests our ICL as a promising recombination layer. Using Kelvin Probe Microscopy (KPM) we measured the work function of the Ag/PFN modified MoO_3. The value of the work function obtained in air turned out to be 4.5 eV, very similar to the one measured under the same conditions for ZnO (4.3 eV). The work function values reported for MoO_3 vary from 6.7 eV for vacuum deposited MoO_3 to 5.5 eV for air exposed MoO_3.[31] Thus, for our ICL, a high work function contrast is expected between the MoO_3 and PFN layers which will further improve the performance of the tandem device.[32]
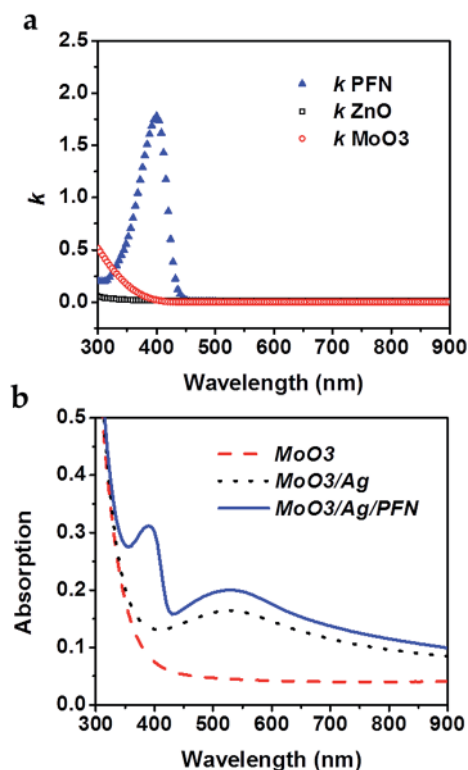
Insight into the key role of the intermediate Ag layer to attain a large FF is provided by analysing a series of devices with varying nominal Ag contents in the ICL. The average FF of these devices increases from an initial value of 50% for the Ag-free ICL to a saturation value of 70–75% for nominal Ag contents of 0.5 nm and above, as can be seen in Fig. 4a. AFM imaging of test glass/ITO/MoO_3 (10 nm)/Ag (0 to 2 nm) samples was performed, revealing that the Ag is distributed within the ICL MoO_3/PFN interface in the form of clusters scattered in a roughly uniform pattern over the MoO_3 layer (Fig. 4b). The average nearest neighbour distance (NND) between Ag particles calculated from the images was found to decrease with increasing Ag content up to 1 nm Ag nominal thickness, when the NND became negligible.

With no Ag in the ICL, electron–hole recombination is not complete, and therefore charges accumulate at the ICL intermediate interface, as evidenced by the S-shape in the corresponding J–V curve (Fig. S8, ESI†). Ag particles attract electrons and holes in the ICL and facilitate their recombination. This results in an enhanced FF for 0.25 nm nominal Ag thickness. For a nominal Ag content of 0.5 nm the average NND is ~10 nm (i.e. the threshold for physical contact between particles has not been reached yet), but the FF has already reached its saturation

Fig. 3   (a) k spectra of ZnO, MoO_3 and PFN electron transporting layers in the 300 nm to 900 nm range. (b) Measured absorbance of the different layers comprising the ICL on glass, 7 nm of MoO_3 alone, MoO_3 and 1 nm of Ag, and finally MoO_3/Ag and 7 nm of PFN.
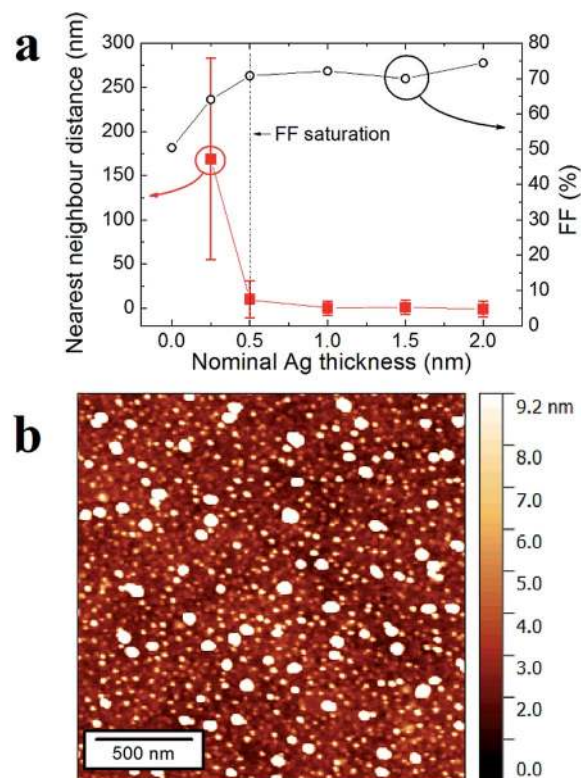

Fig. 4   (a) Average fill factor of tandem cells (black hollow dots) and average nearest neighbor distance between Ag particles in the ICL layer (red solid squares) as a function of the nominal Ag content in the ICL. The vertical dashed line indicates the Ag content for which the FF saturates. Error bars indicate the standard deviations from the average. Solid connecting lines are a guide to the eye. (b) AFM image of a glass/ITO/MoO_3/Ag sample with 0.5 nm nominal Ag thickness. FF is already maximized for the shown Ag particle density.

value, implying that virtually all the recombination in the ICL happens *via* Ag particles. In other words, the maximum FF is achieved just below the percolation threshold for the formation of a long-range connectivity among the Ag clusters corresponding to a deposition of 0.5 nm of Ag. Beyond this point the FF does not seem to increase and further increment of the Ag content up to 2 nm does not imply any improvement in the performance of the cell.

In conclusion, inverted tandem PSCs using PTB7 active layers in both subcells with a MoO_3/Ag/PFN ICL were studied in this work. A PCE of up to 8.2% was achieved with front and rear layer thicknesses around 100 nm and 120 nm, respectively. A FF of 76%, never reported before for an organic tandem solar cell to the best of our knowledge, was also achieved. The total thickness of the ICL is below 20 nm but the PFN is demonstrated to be robust enough to avoid the degradation of the layers underneath. A very thin layer of Ag in the ICL is sufficient for maximizing the FF whilst maintaining a good ICL transparency. The PFN surface modification of the MoO_3/Ag is found to reduce its work function, while maintaining the transparency and the robustness of the ICL. The low absorption spectrum covered by this tandem device appears to leave room for improvement by selecting subcells made of polymers with complementary absorptions.

Experimental section

Device fabrication and materials

PTB7 and PFN were purchased from 1-Material. PC71BM was purchased from ADS. A ZnO precursor, zinc acetate, was purchased from Sigma and MoO_3 from Kurt Lesker. All the materials were used as received. For the single devices, a layer of ZnO or PFN was deposited by spin coating on top of the ITO covered fused silica substrate. ZnO was thermally annealed on a hotplate in air (200 °C, 10 min). The PTB7:PC71BM (1 : 1.5 wt in CB; 3 vol% DIO) layer was deposited by spin coating at 1800 rpm inside a N_2 filled glovebox. Finally, 3 nm MoO_3 and 100 nm Ag layers were used to complete the devices. For the tandem devices, the front subcell was prepared as stated above using ZnO as an ETL. The ICL was fabricated by thermal evaporation of 7 nm of MoO_3 and 0 to 2 nm of Ag followed by the spin coating of PFN (1 mg ml^{-1}) inside the glovebox. The rear subcell was fabricated immediately after PFN deposition following the same steps as for the single junction cells.

Device characterization

J–V curves were measured using a solar simulator under AM1.5 conditions (Abet Technologies, model Sun 3000). EQE values were measured using a QEX10 Quantum Efficiency Measurement System (PV Measurements). The light transmission spectra for the fabricated devices were recorded using an UV-vis-near IR spectrophotometer (Lambda950, PerkinElmer). For the morphology and thickness studies, a Veeco Dimension 3100 AFM operated under ambient conditions in tapping mode was used. A scratching technique was used for accurate measurements of layer thicknesses.[33] Kelvin probe measurements were

performed using an ambient Kelvin Probe system (KP Technologies, Inc.). For the work function studies, an ITO-coated glass substrate was used since this measurement by the Kelvin probe technique requires a conductive substrate. The work function of the tip was calibrated using a gold surface.

Acknowledgements

Notes and references

1 Y. H. Zhou, C. Fuentes-Hernandez, J. Shim, J. Meyer, A. J. Giordano, H. Li, P. Winget, T. Papadopoulos, H. Cheun, J. Kim, M. Fenoll, A. Dindar, W. Haske, E. Najafabadi, T. M. Khan, H. Sojoudi, S. Barlow, S. Graham, J.-L. Bredas, S. R. Marder, A. Kahn and B. Kippelen, *Science*, 2012, **336**, 327.

2 B. Kippelen and J. L. Bredas, *Energy Environ. Sci.*, 2009, **2**, 251.

3 M. Helgesen, R. Sondergaard and F. C. Krebs, *J. Mater. Chem.*, 2010, **20**, 36.

4 C. J. Brabec, S. Gowrisanker, J. J. M. Halls, D. Laird, S. J. Jia and S. P. Williams, *Adv. Mater.*, 2010, **22**, 3839.

5 R. Betancur, P. Romero-Gomez, A. Martinez-Otero, X. Elias, M. Maymo and J. Martorell, *Nat. Photonics*, 2013, **7**, 995.

6 S. B. Darling and F. Youc, *RSC Adv.*, 2013, **3**, 17633.

7 Z. He, C. Zhong, S. Su, M. Xu, H. Wu and Y. Cao, *Nat. Photonics*, 2012, **6**, 591.

8 T. Yang, M. Wang, C. Duan, X. Hu, L. Huang, J. Peng, F. Huang and X. Gong, *Energy Environ. Sci.*, 2012, **5**, 8208.

9 Z. He, C. Zhong, X. Huang, W.-Y. Wong, H. Wu, L. Chen, S. Su and Y. Cao, *Adv. Mater.*, 2011, **23**, 4636.

10 L. Dou, J. You, J. Yang, C.-C. Chen, Y. He, S. Murase, T. Moriarty, K. Emery, G. Li and Y. Yang, *Nat. Photonics*, 2012, **6**, 180.

11 (*a*) Y. Liu, J. Zhao, Z. Li, C. Mu, W. Ma, H. Hu, K. Jiang, H. Lin, H. Ade and H. Yan, *Nat. Commun.*, 2014, **5**, 5293; (*b*) Z. Zheng, S. Zhang, M. Zhang, K. Zhao, L. Ye, Y. Chen, B. Yang and J. H. Hou, *Adv. Mater.*, 2014, **27**, 1189.

12 T. Ameri, G. Dennler, C. Lungenschmied and C. J. Brabec, *Energy Environ. Sci.*, 2009, **2**, 347.

13 J. You, L. Dou, K. Yoshimura, T. Kato, K. Ohya, T. Moriarty, K. Emery, C.-C. Chen, J. Gao, G. Li and Y. Yang, *Nat. Commun.*, 2013, **4**, 1446.

14 D. Dou, J. You, Z. Hong, Z. Xu, G. Li, R. A. Street and Y. Yang, *Adv. Mater.*, 2013, **46**, 6642.

15 T. Ameri, N. Li and C. J. Brabec, *Energy Environ. Sci.*, 2013, **6**, 2390.

16 G. Dennler, M. C. Scharber, T. Ameri, P. Denk, K. Forberich, C. Waldauf and C. J. Brabec, *Adv. Mater.*, 2008, **20**, 579.

17 N. Li, D. Baran, G. D. Spyropoulos, H. Zhang, S. Berny, M. Turbiez, T. Ameri, F. C. Krebs and C. J. Brabec, *Adv. Energy Mater.*, 2014, **4**, 1400084.

18 X. Guo, N. Zhou, S. J. Lou, J. Smith, D. B. Tice, J. W. Hennek, R. P. Ortiz, J. T. L. Navarrete, S. Li, J. Strzalka, L. X. Chen, R. P. H. Chang, A. Facchetti and T. J. Marks, *Nat. Photonics*, 2013, **7**, 825.

19 B. Qi and J. Wang, *Phys. Chem. Chem. Phys.*, 2013, **15**, 8972.

20 (*a*) V. D. Mihailetchi, H. Xie, B. de Boer, L. J. A. Koster and P. W. M. Blom, *Adv. Funct. Mater.*, 2006, **16**, 699; (*b*) A. Gadisa, F. Zhang, D. Sharma, M. Svensson, M. R. Adnersson and O. Inganäs, *Thin Solid Films*, 2007, **15**, 3126; (*c*) B. Ray and M. A. Alam, *Sol. Energy Mater. Sol. Cells*, 2012, **99**, 204.

21 W. Chen, M. P. Nikiforova and S. B. Darling, *Energy Environ. Sci.*, 2012, **5**, 8045.

22 (*a*) M. D. Irwin, D. B. Buchholz, A. W. Hains, R. P. H. Chang and T. J. Marks, *Proc. Natl. Acad. Sci. U. S. A.*, 2008, **105**, 2783; (*b*) J. Yu, Y. Zang, H. Li and J. Huang, *Thin Solid Films*, 2012, **520**, 6653; (*c*) T. Stubhan, M. Salinas, A. Ebel, F. C. Krebs, A. Hirsch, M. Halik and C. J. Brabec, *Adv. Energy Mater.*, 2012, **2**, 532.

23 Y. Yuan, J. Huang and G. Li, *Green*, 2011, **1**, 65.

24 A. Martínez-Otero, X. Elias, R. Betancur and J. Martorell, *Adv. Opt. Mater.*, 2013, **1**, 37.

25 R. Betancur, A. Martínez-Otero, X. Elias, P. Romero Gómez, S. Colodrero, H. Miguez and J. Martorell, *Sol. Energy Mater. Sol. Cells*, 2012, **104**, 87.

26 J. Jo, J.-R. Pouliot, D. Wynands, S. D. Collins, J. Y. Kim, T. L. Nguyen, H. Y. Woo, Y. Sun, M. Leclerc and A. J. Heeger, *Adv. Mater.*, 2013, **25**, 4783.

27 L. Lu and L. Yu, *Adv. Mater.*, 2014, **26**, 4413.

28 J. You, C.-C. Chen, Z. Hong, K. Yoshimura, K. Ohya, R. Xu, S. Ye, J. Gao, G. Li and Y. Yang, *Adv. Mater.*, 2013, **25**, 3973.

29 P. Romero-Gomez, R. Betancur, A. Martínez-Otero, X. Elias, M. Mariano, B. Romero, B. Arredondo, R. Vergaz and J. Martorell, *Sol. Energy Mater. Sol. Cells*, 2015, **137**, 44.

30 (*a*) G. Dennler, K. Forberich, T. Ameri, C. Waldauf, P. Denk, C. J. Brabec, K. Hingerl and A. J. Heeger, *J. Appl. Phys.*, 2007, **102**, 123109; (*b*) N. Li, T. Stubhan, D. Baran, J. Min, H. Wang, T. Ameri and C. J. Brabec, *Adv. Energy Mater.*, 2013, **3**, 301; (*c*) N.-K. Persson and O. Ingana, *Sol. Energy Mater. Sol. Cells*, 2006, **90**, 3491.

31 (*a*) S. Murase and Y. Yang, *Adv. Mater.*, 2012, **24**, 2459; (*b*) J. Meyer, S. Hamwi, M. Kröger, W. Kowalsky, T. Riedl and A. Kahn, *Adv. Mater.*, 2012, **24**, 5408.

32 (*a*) Y. Zhou, C. Fuentes-Hernandez, J.-W. Shim, T.-M. Khan and B. Kippelen, *Energy Environ. Sci.*, 2012, **5**, 9827; (*b*) J.-W. Shim, C. Fuentes-Hernandez, Y. Zhou, A. Dindar, T.-M. Khan, A.-J. Giordano, H. Cheun, M. Yun, S.-R. Marder and B. Kippelen, *Adv. Energy Mater.*, 2014, **4**, 1400048.

33 A. Martínez-Otero, F. Busqué, J. Hernando and D. Ruiz-Molina, *Nanoscale*, 2010, **2**, 1781.